PHYSICAL REVIEW B **93**, 060506(R) (2016)

Nodeless superconductivity in noncentrosymmetric $PbTaSe_2$ single crystals

G. M. Pang,[1] M. Smidman,[1] L. X. Zhao,[2] Y. F. Wang,[1] Z. F. Weng,[1] L. Q. Che,[1] Y. Chen,[1] X. Lu,[1,3] G. F. Chen,[2,4] and H. Q. Yuan[1,3,*]

[1]*Center for Correlated Matter and Department of Physics, Zhejiang University, Hangzhou 310058, China*

[2]*Beijing National Laboratory for Condensed Matter Physics, Institute of Physics, Chinese Academy of Sciences, Beijing 100190, China*

[3]*Collaborative Innovation Center of Advanced Microstructures, Nanjing 210093, China*

[4]*Collaborative Innovation Center of Quantum Matter, Beijing 100084, China*

(Received 13 December 2015; published 5 February 2016)

We report an investigation of the superconducting order parameter of the noncentrosymmetric compound $PbTaSe_2$, which is believed to have a topologically nontrivial band structure. Precise measurements of the London penetration depth $\Delta\lambda(T)$ obtained using a tunnel diode oscillator (TDO) based method show an exponential temperature dependence at $T \ll T_c$, suggesting a nodeless superconducting gap structure. A single-gap s-wave model well describes the corresponding normalized superfluid density $\rho_s(T)$, with a gap magnitude of $\Delta(0) \simeq 1.88T_c$. This is very close to the value of $1.76T_c$ for weak-coupling BCS superconductors, indicating conventional fully-gapped superconductivity in $PbTaSe_2$.

DOI: 10.1103/PhysRevB.93.060506

Noncentrosymmetric superconductors (NCS), where the crystal structure does not have a center of inversion, display unique properties. In the presence of antisymmetric spin-orbit coupling (ASOC), the pairing state is expected to be a mixture of spin singlet and triplet components, leading to unusual properties, even when the pairing has the conventional electron-phonon mechanism [1,2]. For instance, evidence for nodal superconductivity has been found in the weakly correlated NCS Li_2Pt_3B and Y_2C_3 [3,4]. Other NCS such as $LaNiC_2$ and BiPd, have been suggested to be multigap superconductors, which gives an indication of singlet-triplet mixing, although this may also arise in a purely singlet s-wave channel [5–7]. Despite the anticipation of mixed parity pairing in NCS, single-gap BCS-like superconductivity is clearly observed in many of these materials, such as Re_3W, $LaRhSi_3$, and $BaPtSi_3$ [8–10]. The presence of singlet-triplet mixing has also been probed by looking for an anisotropic spin susceptibility via measurements of the upper critical field (H_{c2}) and Knight shift, as in the case of $CeRhSi_3$ and $CeIrSi_3$ [11,12]. In addition, NCS were also proposed to be good candidates for topological superconductivity [13], and there has been particular interest due to the possibility of gapless edge states and Majorana fermions [14,15].

Recently, the new NCS $PbTaSe_2$ has been the focus of much interest. The compound crystallizes in a noncentrosymmetric structure (space group $P\bar{6}m2$), containing hexagonal $TaSe_2$ layers [16]. The resistivity $\rho(T)$ of $TaSe_2$ shows a charge-density-wave (CDW) transition at around 122 K, which is gradually suppressed upon doping with Pb and pure $PbTaSe_2$ becomes superconducting below $T_c = 3.7$ K [17,18]. Meanwhile, the inversion symmetry of the crystal structure is also broken as a result of intercalation with Pb, making $PbTaSe_2$ a new NCS. Detailed comparisons between electronic structure calculations and angle resolved photoemission spectroscopy (ARPES) measurements reveal the presence of topological nodal lines in the band structure, near the Fermi level [19]. This is a result of the spin-orbit coupling lifting the degeneracy of the conduction and valence bands, except at the nodal positions which are gapless due to the reflection symmetry of the crystal lattice. In addition, ARPES measurements give evidence for Dirac surface states, and it was suggested that this may allow for the presence of Majorana bound states in the vortex cores of $PbTaSe_2$ [20].

It is therefore of interest to determine whether there is any interplay between the topologically nontrivial band structure and the superconductivity. To find out whether this is a candidate for topological superconductivity, it is important to characterize the superconducting order parameter of $PbTaSe_2$ through measurements of the bulk properties. In this Rapid Communication, we report the temperature dependence of the change of London penetration depth $\Delta\lambda(T)$ of high quality single crystal samples using a tunnel diode oscillator (TDO) based method. We find that exponential behavior is clearly observed at $T \ll T_c$, implying a nodeless superconducting energy gap. Further analysis reveals that both $\Delta\lambda(T)$ and the derived superfluid density $\rho_s(T)$ can be best fitted by an s-wave model, with a gap size close to the BCS value of $1.76T_c$, providing strong evidence for single-gap, weak-coupling nodeless superconductivity in the bulk of $PbTaSe_2$.

Single crystals of $PbTaSe_2$ were synthesized using a chemical vapor transport (CVT) process [19]. The temperature dependence of the electrical resistivity $\rho(T)$ was measured in a ^{4}He system from 292 K to about 3 K, using a four-probe method. Measurements of the dc-magnetic susceptibility were performed in a superconducting quantum interference device (SQUID) magnetometer (MPMS-5T) in the temperature range of 2–6 K, with both field-cooling (FC) and zero-field-cooling (ZFC) in a small applied magnetic field of 10 Oe.

The temperature dependence of the change in London penetration depth $\Delta\lambda(T)$ was precisely measured down to a base temperature of 0.35 K in a ^{3}He cryostat using a TDO-based technique [21] with an operating frequency of about 7 MHz and a noise level of about 0.1 Hz. Single crystal samples were cut into rectangular plates, with dimensions of (500–900) × (500–900) × (5–10) μm^3. The samples were mounted on a sapphire rod and inserted into the TDO coil without making contact, and the resonant frequency of the

*hqyuan@zju.edu.cn

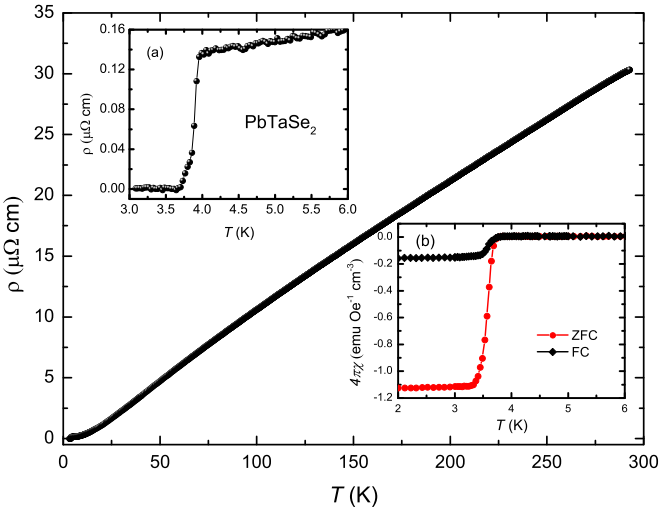

FIG. 1. The main panel shows the electrical resistivity $\rho(T)$ of $PbTaSe_2$ single crystals from room temperature down to around 3 K. The insets show the low temperature behavior of (a) $\rho(T)$ and (b) magnetic susceptibility $4\pi\chi$ with a field applied in the ab plane, where sharp superconducting transitions are observed.

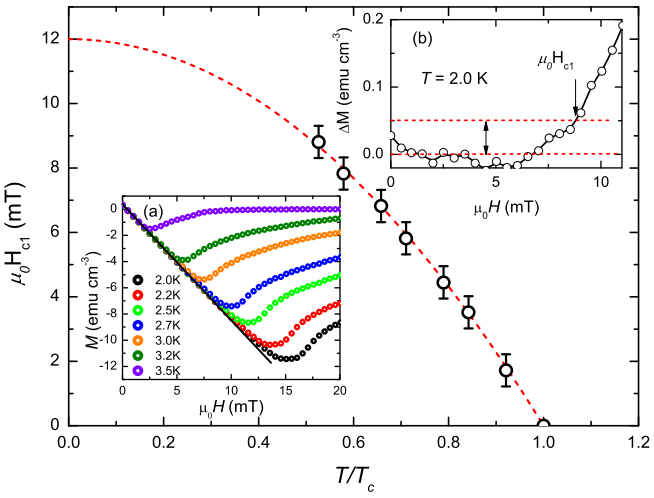

FIG. 2. Temperature dependence of the lower critical field $\mu_0 H_{c1}$ of $PbTaSe_2$, defined as the field above which the field dependence of the magnetization $M(H)$ deviates from a linear decrease. The dashed red line shows a fit to the Ginzburg-Landau formula $H_{c1}(T) = H_{c1}(0)(1-(T/T_c)^2)$. Inset (a) shows $M(H)$ for fields applied in the ab plane, at various temperatures in the superconducting state. Inset (b) shows the deviation ΔM of the $M(H)$ data from linear behavior at 2 K. H_{c1} is taken to be the field where the deviation is greater than 0.05 emu cm^{-3}, above the region enclosed by the dashed lines.

TDO circuit [$f(T)$] was measured as a function of temperature. A tiny ac field of about 20 mOe was applied to the sample using the TDO coil, which is much smaller than the lower critical field H_{c1}, guaranteeing that the sample is entirely in the Meissner state and therefore the obtained $\Delta\lambda(T)$ can be regarded as the change of the London penetration depth. This quantity is proportional to $\Delta f(T)$ the change in $f(T)$ from the zero temperature value, with $\Delta\lambda(T) = G\Delta f(T)$, where the calibration constant G is determined from the sample and coil geometry, following Ref. [22].

Single crystals of $PbTaSe_2$ were characterized using both resistivity and magnetic susceptibility measurements, as shown in Fig. 1. The temperature dependence of $\rho(T)$ displays metallic behavior, since it decreases upon cooling the sample from room temperature, with a very small residual resistivity of about 0.14 $\mu\Omega$ cm, just above the superconducting transition. As a result there is a large residual resistivity ratio (RRR) of $\rho(292\,\mathrm{K})/\rho(4\,\mathrm{K}) = 220$, which demonstrates the high quality of the single crystals. Upon following the method in Ref. [23], using a coherence length of $\xi = 16.2$ nm and a normal state Sommerfeld coefficient $\gamma_n = 4.8$ mJ/mol K^2 [24], the small residual resistivity gives rise to a large mean free path of 10 μm. This is significantly larger than the coherence length, indicating that the sample is in the clean limit. The presence of a superconducting transition is clearly displayed in the insets of Fig. 1, onsetting at around 3.9 K in the resistivity and the magnetic susceptibility shows a clear diamagnetic signal, suggesting bulk superconductivity in $PbTaSe_2$. Here, the magnetic susceptibility slightly drops below the value of -1 for full diamagnetic shielding, which is likely due to demagnetization effects.

In inset (a) of Fig. 2, the field dependence of the magnetization is displayed, with the field applied in the ab plane. In the case of type-II superconductors, the magnetization $M(H)$ usually decreases linearly with increasing applied magnetic field for $\mu_0 H < \mu_0 H_{c1}$, where $\mu_0 H_{c1}$ is the lower critical field, below which the sample is in the Meissner state. When $\mu_0 H > \mu_0 H_{c1}$, $M(H)$ deviates from linear behavior, due to the formation of vortices in the mixed state. We measured from zero field up to 20 mT at different temperatures in the superconducting state. The values of $\mu_0 H_{c1}$ were obtained from the field where the deviation $[\Delta M(H)]$ from linear behavior $[M_{\mathrm{lin}}(H)]$ is greater than 0.05 emu cm^{-3}, where $\Delta M(H) = M(H) - M_{\mathrm{lin}}(H)$. This is displayed for the data at 2 K in inset (b) of Fig. 2.

The temperature dependence of $\mu_0 H_{c1}$ is shown in the main panel of Fig. 2. The zero temperature lower critical field $\mu_0 H_{c1}(0) = 12.0$ mT was estimated from fitting $H_{c1}(T) = H_{c1}(0)(1-(T/T_c)^2)$, as shown by the red-dashed line in the figure. In Ginzburg-Landau theory, the magnetic penetration depth λ is related to both the coherence length ξ and lower critical field $\mu_0 H_{c1}$, as described by $\mu_0 H_{c1} = \Phi_0/(4\pi\lambda^2)\ln(\lambda/\xi + 1/2)$, where Φ_0 is the magnetic flux quantum [25]. Using the values of $\mu_0 H_{c1}(0) = 12.0$ mT and $\xi = 16.2$ nm mentioned previously, $\lambda(0) = 204$ nm was estimated and this value was used to calculate the superfluid density below. In addition, $\lambda(T)$ was estimated using the obtained values of $\mu_0 H_{c1}(T)$, where $\xi(T)$ was calculated from the reported values of $H_{c2}(T)$ [24,26].

The penetration depth of two samples is shown in Fig. 3, with calibration factors of $G = 8.0$ Å/Hz and 10.0 Å/Hz for samples #1 and #2, respectively. The change of the London penetration depth as a function of temperature $\Delta\lambda(T)$ is shown for sample #1 in the inset of Fig. 3 from 5 K above T_c, down to about 0.35 K. A sharp decrease near 3.9 K indicates the onset of superconductivity, in agreement with the resistivity and susceptibility measurements and confirms the high sample quality. The main panel of Fig. 3 displays the low temperature

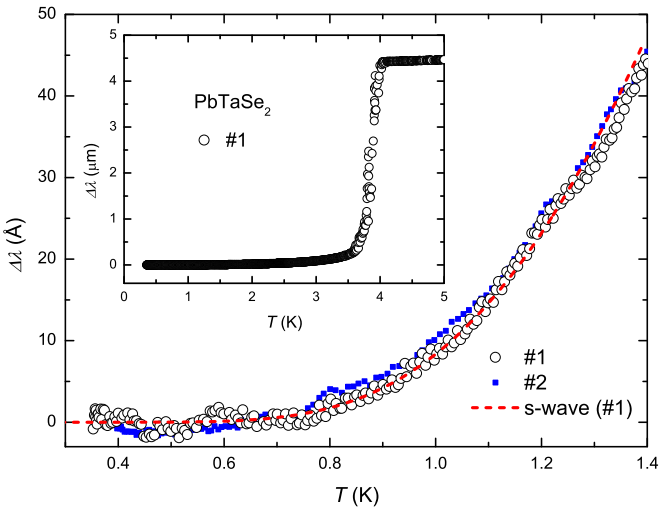

FIG. 3. The change of the London penetration depth in the ab plane $\Delta\lambda(T)$ as a function of temperature below $T_c/3$ for two samples of single crystal $PbTaSe_2$. The solid line shows a fit to an s-wave model described in the text, which indicates conventional fully-gapped superconductivity. The inset shows $\Delta\lambda(T)$ from 5 K down to the base temperature for sample #1, which exhibits a sharp superconducting transition around 3.9 K, consistent with resistivity and magnetic susceptibility measurements.

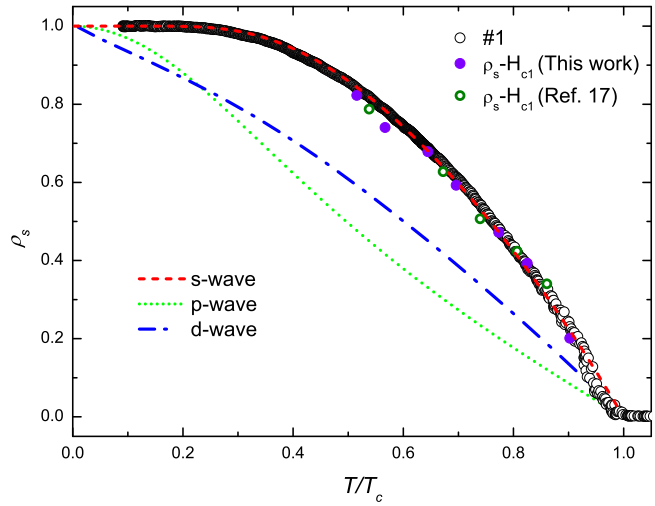

FIG. 4. Temperature dependence of the normalized superfluid density $\rho_s(T)$ for sample #1 of single crystal $PbTaSe_2$. The symbols represent the experimental data while the lines show the results of fitting the data with different models of the gap structure. The solid violet and open green circles show $\rho_s(T)$ obtained from our $\mu_0 H_{c1}$ measurements and the data in Ref. [17], respectively.

measurements of both samples below 1.4 K, where $\Delta\lambda(T)$ rapidly decreases upon cooling, before flattening below about 0.8 K, which suggests fully gapped superconductivity and the absence of low energy excitations. As shown in the plot, this behavior is well reproducible between the two samples. For an s-wave superconductor at $T \ll T_c$, $\lambda(T)$ can be approximated using

$$\Delta\lambda(T) = \lambda(T) - \lambda(0) = \lambda(0)\sqrt{\frac{\pi\Delta(0)}{2T}}\exp\left(-\frac{\Delta(0)}{T}\right), \quad (1)$$

where $\Delta(0)$ is the superconducting gap magnitude in units such that $k_B = 1$ [27]. The data for sample #1 was fitted and the solid line in the figure shows that this expression gives excellent agreement with the experimental data below $T_c/3$, with a value of $\Delta(0) = 1.72T_c$, while a very similar value of $\Delta(0) = 1.70T_c$ is obtained from fitting sample #2, both consistent with weakly coupled BCS superconductivity in $PbTaSe_2$.

To further characterize the superconducting gap symmetry of $PbTaSe_2$, we also analyzed the normalized superfluid density $\rho_s(T)$, which was converted from $\Delta\lambda(T)$ using $\rho_s(T) = \lambda(0)^2/\lambda(T)^2$, with $\lambda(0) = 204$ nm and is displayed for sample #1 in Fig. 4. In addition, we have plotted $\rho_s(T)$ calculated from $\lambda(T)$ obtained both from our values of $\mu_0 H_{c1}(T)$ and from the data in Ref. [17], which are consistent with $\rho_s(T)$ obtained from the TDO measurements. For a given gap function Δ_k, $\rho_s(T)$ can be calculated as:

$$\rho_s(T) = 1 + 2\left\langle \int_{\Delta_k}^{\infty} \frac{E\,dE}{\sqrt{E^2 - \Delta_k^2}} \frac{\partial f}{\partial E} \right\rangle_{FS}, \quad (2)$$

where $f(E,T) = [1 + \exp(E/T)]^{-1}$ is the Fermi distribution function and $\langle \ldots \rangle_{FS}$ represents an average over the Fermi surface [27]. Here, the gap function is defined as $\Delta_k(T) = \Delta(T)g_k$, where g_k contains the angular dependence and $g_k = 1$, $\sin\theta$ and $\cos 2\phi$ for the s-, p- and d-wave models, respectively, where θ is the polar angle and ϕ is the azimuthal angle. The temperature dependence of the gap $[\Delta(T)]$ is approximated as

$$\Delta(T) = \Delta(0)\tanh\{1.82[1.018(T_c/T - 1)]^{0.51}\}, \quad (3)$$

where $\Delta(0)$ represents the gap magnitude at zero temperature, which is the only adjustable parameter in the fitting [28].

The fitting results are also plotted in Fig. 4. In the case of the s-wave model, the superconducting gap is isotropic. It is clearly shown that the experimental data is well fitted by this model, with a gap amplitude of $\Delta(0) = 1.88T_c$. This is consistent with the value obtained from fitting the penetration depth, close to the BCS value, suggesting that $PbTaSe_2$ is a fully-gapped, weakly coupled superconductor. On the other hand, a p-wave model with point nodes and a d-wave model with line nodes were also used for comparison, both of which predict ρ_s to continue increasing with decreasing temperature due to the existence of low energy excitations. These models strongly disagree with our results, giving further evidence for nodeless superconductivity in $PbTaSe_2$.

Our results indicate that the bulk superconductivity of $PbTaSe_2$ is consistent with fully gapped s-wave superconductivity with a gap size close to the weakly coupled BCS value. The nodeless bulk superconductivity is consistent with recent measurements of the specific heat, which could also be fitted with exponential behavior at low temperatures [24]. However, different strengths of the electron-phonon coupling were deduced, with strongly coupled behavior suggested from the large specific heat jump $\Delta C/\gamma T_c$ in Ref. [24], while the values in Refs. [17,29] are consistent with weak coupling, in line with our results. In addition, thermal conductivity measurements also indicate nodeless superconductivity [30] and it was also suggested that the "S" shape in the field dependence of the

thermal conductivity may indicate multiband superconductivity in $PbTaSe_2$. However, from our measurements we find that the superfluid density can be well accounted for by a single gap model.

The fact that these results are consistent with single-gap s-wave superconductivity would suggest that the pairing in noncentrosymmetric $PbTaSe_2$ is dominated by the spin singlet component. Indeed the lack of singlet-triplet mixing in $PbTaSe_2$ is somewhat of a puzzle, given the strong effect of the ASOC [19]. It should be noted that there are other NCS which are compatible with single-gap, BCS-like superconductivity, including materials such as $LaPt_3Si$ which show a significant ASOC [31], and the reason for this behavior has yet to be resolved. It has previously been suggested that for NCS to have gapless edge states and Majorana modes, the triplet component should be larger than the s-wave singlet component [14]. For s-wave superconductors in the presence of Rashba ASOC, it is necessary to apply a large magnetic field for Majorana fermions to be realized [15]. Nevertheless, it was suggested in Ref. [20] that the topologically nontrivial nature of the electronic structure of $PbTaSe_2$ means that Majorana modes may be present in vortices, even if the bulk superconductivity is of an s-wave nature, as long as it is fully gapped. Given that our results support the existence of fully gapped superconductivity, further experiments are desirable to look for the presence of Majorana modes and other signatures of topological order.

To summarize, we have investigated the superconducting order parameter of the noncentrosymmetric superconductor $PbTaSe_2$. The change in the London penetration depth $\Delta\lambda(T)$ of single crystals was precisely measured down to $0.1T_c$, which clearly shows an exponential temperature dependence below $T_c/3$, indicating fully gapped behavior. Both $\Delta\lambda(T)$ and its deduced superfluid density $\rho_s(T)$ can be described by a single-gap s-wave model, providing strong evidence for a nodeless superconducting gap structure in $PbTaSe_2$. A gap magnitude of $\Delta(0) = 1.88T_c$ is obtained from fitting the superfluid density, which is slightly larger than the weak coupling BCS value of $1.76T_c$ and indicates the absence of strong electron-phonon coupling.

We thank C. Cao, S. H. Pan, D. L. Feng, and D. F. Agterberg for interesting discussions. This work was supported by the National Basic Research Program of China (Grant No. 2011CBA00103), the National Natural Science Foundation of China (Grant No. 11474251 and No. 11174245), and the Fundamental Research Funds for the Central Universities.

[1] L. P. Gor'kov and E. I. Rashba, Superconducting 2D System with Lifted Spin Degeneracy: Mixed Singlet-Triplet State, Phys. Rev. Lett. **87**, 037004 (2001).

[2] P. A. Frigeri, D. F. Agterberg, A. Koga, and M. Sigrist, Superconductivity without Inversion Symmetry: MnSi Versus $CePt_3Si$, Phys. Rev. Lett. **92**, 097001 (2004).

[3] H. Q. Yuan, D. F. Agterberg, N. Hayashi, P. Badica, D. Vandervelde, K. Togano, M. Sigrist, and M. B. Salamon, S-Wave Spin-Triplet Order in Superconductors without Inversion Symmetry: Li_2Pd_3B and Li_2Pt_3B, Phys. Rev. Lett. **97**, 017006 (2006).

[4] J. Chen, M. B. Salamon, S. Akutagawa, J. Akimitsu, J. Singleton, J. L. Zhang, L. Jiao, and H. Q. Yuan, Evidence of nodal gap structure in the noncentrosymmetric superconductor Y_2C_3, Phys. Rev. B **83**, 144529 (2011).

[5] M. Mondal, B. Joshi, S. Kumar, A. Kamlapure, S. C. Ganguli, A. Thamizhavel, S. S. Mandal, S. Ramakrishnan, and P. Raychaudhuri, Andreev bound state and multiple energy gaps in the noncentrosymmetric superconductor BiPd, Phys. Rev. B **86**, 094520 (2012).

[6] L. Jiao, J. L. Zhang, Y. Chen, Z. F. Weng, Y. M. Shao, J. Y. Feng, X. Lu, B. Joshi, A. Thamizhavel, S. Ramakrishnan, and H. Q. Yuan, Anisotropic superconductivity in noncentrosymmetric BiPd, Phys. Rev. B **89**, 060507(R) (2014).

[7] J. Chen, L. Jiao, J. L. Zhang, Y. Chen, L. Yang, M. Nicklas, F. Steglich, and H. Q. Yuan, Evidence for two-gap superconductivity in the non-centrosymmetric compound $LaNiC_2$, New J. Phys. **15**, 053005 (2013).

[8] P. K. Biswas, A. D. Hillier, M. R. Lees, and D. McK. Paul, Comparative study of the centrosymmetric and noncentrosymmetric superconducting phases of Re_3W using muon spin spectroscopy and heat capacity measurements, Phys. Rev. B **85**, 134505 (2012).

[9] V. K. Anand, A. D. Hillier, D. T. Adroja, A. Strydom, H. Michor, K. A. McEwen, and B. D. Rainford, Specific heat and μSR study on the noncentrosymmetric superconductor $LaRhSi_3$, Phys. Rev. B **83**, 064522 (2011).

[10] E. Bauer, R. T. Khan, H. Michor, E. Royanian, A. Grytsiv, N. Melnychenko-Koblyuk, P. Rogl, D. Reith, R. Podloucky, E. W. Scheidt, W. Wolf, and M. Marsman, $BaPtSi_3$: A noncentrosymmetric BCS-like superconductor, Phys. Rev. B **80**, 064504 (2009).

[11] N. Kimura, K. Ito, H. Aoki, S. Uji, and T. Terashima, Extremely High Upper Critical Magnetic Field of the Noncentrosymmetric Heavy Fermion Superconductor $CeRhSi_3$, Phys. Rev. Lett. **98**, 197001 (2007).

[12] H. Mukuda, T. Ohara, M. Yashima, Y. Kitaoka, R. Settai, Y. Ōnuki, K. M. Itoh, and E. E. Haller, Spin Susceptibility of Noncentrosymmetric Heavy-Fermion Superconductor $CeIrSi_3$ under Pressure: Si^{29} Knight-Shift Study on Single Crystal, Phys. Rev. Lett. **104**, 017002 (2010).

[13] X.-L. Qi, T. L. Hughes, and S. C. Zhang, Topological invariants for the Fermi surface of a time-reversal-invariant superconductor, Phys. Rev. B **81**, 134508 (2010).

[14] M. Sato and S. Fujimoto, Topological phases of noncentrosymmetric superconductors: Edge states, Majorana fermions, and non-Abelian statistics, Phys. Rev. B **79**, 094504 (2009).

[15] M. Sato, Y. Takahashi, and S. Fujimoto, Non-Abelian topological orders and Majorana fermions in spin-singlet superconductors, Phys. Rev. B **82**, 134501 (2010).

[16] V. Vescoli, L. Degiorgi, H. Berger, and L. Forró, Dynamics of Correlated Two-Dimensional Materials: The $2H$-$TaSe_2$ Case, Phys. Rev. Lett. **81**, 453 (1998).

[17] M. N. Ali, Q. D. Gibson, T. Klimczuk, and R. J. Cava, Noncentrosymmetric superconductor with a bulk three-dimensional

Dirac cone gapped by strong spin-orbit coupling, Phys. Rev. B **89**, 020505 (2014).

[18] A. Sharafeev, R. Sankar, A. Glamazda, K. Y. Choi, R. Bohle, P. Lemmens, and F. C. Chou, Doping effects on charge density instability in non-centrosymmetric Pb_xTaSe_2, arXiv:1505.00748.

[19] G. Bian, T.-R. Chang, R. Sankar, S.-Y. Xu, H. Zheng, T. Neupert, C.-K. Chiu, S.-M Huang, G. Q. Chang, I. Belopolski *et al.*, Topological Nodal-Line Fermions in the Non-Centrosymmetric Superconductor Compound $PbTaSe_2$, arXiv:1505.03069.

[20] T.-R. Chang *et al.*, Topological Dirac States and Pairing Correlations in the Non-Centrosymmetric Superconductor $PbTaSe_2$, arXiv:1511.06231.

[21] C. T. Van Degrift, Tunnel diode oscillator for 0.001 ppm measurements at low temperatures, Rev. Sci. Instrum. **46**, 599 (1975).

[22] R. Prozorov, R. W. Giannetta, A. Carrington, and F. M. Araujo-Moreira, Meissner-London state in superconductors of rectangular cross section in a perpendicular magnetic field, Phys. Rev. B **62**, 115 (2000).

[23] T. P. Orlando, E. J. McNiff, S. Foner, and M. R. Beasley, Critical fields, Pauli paramagnetic limiting, and material parameters of Nb_3Sn and V_3Si, Phys. Rev. B **19**, 4545 (1979).

[24] C. L. Zhang, Z. J. Yuan, S. Y. Xu, X. Zhang, M. Z. Hasan, and S. Jia, Exotic Superconducting Properties in Topological Nodal Semimetal $PbTaSe_2$, arXiv:1511.04673.

[25] E. H. Brandt, Properties of the ideal Ginzburg-Landau vortex lattice, Phys. Rev. B **68**, 054506 (2003).

[26] J. R. Wang *et al.*, Upward curvature of the upper critical field and the V-Shaped pressure dependence of T_c in the noncentrosymmetric superconductor $PbTaSe_2$, J. Supercond. Nov. Magn. **28**, 3173 (2015).

[27] R. Prozorov and R. W. Giannetta, Magnetic penetration depth in unconventional superconductors, Supercond. Sci. Technol. **19**, R41 (2006).

[28] A. Carrington and F. Manzano, Magnetic penetration depth of MgB_2, Physica C **385**, 205 (2003).

[29] R. Sankar, G. N. Rao, I. P. Muthuselvam, G. Bian, H. Zheng, G. P.-J. Chen, T. R. Chang, S. Y. Xu, G. S. Murgan, and C. H. Lin *et al.*, Single crystal growth and physical property characterization of $PbTaSe_2$ as a noncentrosymmetric type-II superconductor, arXiv:1511.05295.

[30] M. X. Wang, Y. Xu, L. P. He, J. Zhang, X. C. Hong, P. L. Cai, Z. B. Wang, J. K. Dong, and S. Y. Li, Nodeless superconducting gaps in noncentrosymmetric superconductor $PbTaSe_2$ with topological bulk nodal lines, Phys. Rev. B **93**, 020503(R) (2016).

[31] T. Takeuchi, T. Yasuda, M. Tsujino, H. Shishido, R. Settai, H. Harima, and Y. Ōnuki, Specific heat and de Haas–van Alphen experiments on the heavy-Fermion superconductor $CePt_3Si$, J. Phys. Soc. Jpn. **76**, 014702 (2007).